HHS Public Access

Author manuscript

Adv Mater. Author manuscript; available in PMC 2016 July 08.

Published in final edited form as:

Adv Mater. 2015 July 8; 27(26): 3947–3952. doi:10.1002/adma.201501329.

Simultaneous nano- and micro-scale control of nanofibrous microspheres self-assembled from star-shaped polymers

Zhanpeng Zhang[1], **Ryan L. Marson**[2,3], **Zhishen Ge**[4], **Sharon C. Glotzer**[2,3,5,6], and **Peter X. Ma**[1,2,4,6,*]

[1]Department of Biomedical Engineering, University of Michigan, Ann Arbor, MI, 48109-1078

[2]Materials Science and Engineering, University of Michigan, Ann Arbor, MI, 48109-1078

[3]Biointerfaces Institute, University of Michigan, Ann Arbor, MI, 48109-1078

[4]Department of Biologic and Materials Sciences, University of Michigan, Ann Arbor, MI, 48109-1078

[5]Department of Chemical Engineering, University of Michigan, Ann Arbor, MI, 48109-1078

[6]Macromolecular Science and Engineering Center, University of Michigan, Ann Arbor, MI, 48109-1078

Abstract

The mechanism underlying the multi-scale self-assembly of star-shaped polymers into non-hollow, hollow, and spongy nanofibrous microspheres is reported. Star-shaped poly(L-lactic acid) polymers with varying arm-numbers and arm-lengths are synthesized, dissolved in tetrahydrofuran, emulsified in glycerol, and thermally-induced to phase separate, resulting in microspheres that are either smooth or fibrous on the nano-scale, and either non-hollow, hollow, or spongy on the micro-scale. Molecular architecture and the hydroxyl density are shown to control assembly and morphology at both nano- and micro-scales. Nanofibers form only when the arm length is sufficiently long, while an increase in hydroxyl density causes the microspheres to change from non-hollow to hollow to spongy. We demonstrate via both experiments of capping or doubling the hydroxyl end groups and dissipative particle dynamics simulations that the affinity of hydroxyl to glycerol is critical to stabilizing the micro-scale structure. A “phase diagram” was constructed for the six types of microspheres in relation to the molecular structures of the star-shaped polymers. The proposed mechanism explains how star-shaped polymers self-assemble into various microspheres, and guides us to simultaneously control both nano- and micro-features of the microspheres.

Keywords

star-shaped polymer; self-assembly; simulation; biomaterials; nanofibrous microspheres

[*]To whom correspondence should be addressed: Peter X. Ma, Ph.D., Professor, Department of Biologic and Materials Sciences, The University of Michigan, 1011 North University Ave., Room 2211, Ann Arbor, MI 48109-1078, Tel: (734) 764-2209, Fax: (734) 647-2110, mapx@umich.edu.

Supporting Information

Supporting Information is available from the Wiley Online Library.

Spherical micro- and nano-structured particles are important elements of many current and future technologies, including delivery of chemical and biological molecules [1], fabrication of electronic displays [2], preparation of photonic [3], plasmonic [4], and photosynthetic [5] assemblies and self-healing structural materials [6], as well as separation, sensing and catalysis [7]. The external and internal structures of the microsphere are critical to their function and performance. For tissue regeneration, a porous structure on the micrometer scale can increase cell-loading efficiency, improve nutrition transport, decrease the amount of degradation products, and facilitate vascularization and tissue formation [8]. On the nanometer scale, a nanofibrous structure mimics the structure of collagen and improves cell-matrix interactions [9]. Recently, unusual nanofibrous, hollow microspheres were synthesized from star-shaped poly(L-lactic acid) (SS-PLLA), which integrated both a fibrous nanostructure and a hollow microstructure for the first time [10]. However, the underlying mechanism of the nanofibrous hollow microsphere formation was unclear. In this study, we demonstrate via experiments and computer simulations how the molecular structure of SS-PLLA dictates its self-assembly on both the nano- and micro-meter scales, and we describe a versatile method to prepare microspheres with simultaneously controlled nano- and microstructures.

To study how the molecular architecture of star-shaped polymers affects assembly, we choose initiators with X initiating sites (hydroxyls (OH)) to polymerize L-lactide (LLA) to generate star-shaped poly(L-lactic acid) (SS-PLLA) with q arms (X = 2, 3, 4, 8, 16, 32 and 64, Figure S1). The theoretical arm length is calculated from the feeding ratio, LLA:OH (=Y). The actual average arm length N is determined by ^{1}H-NMR. It should be noted that the q<X and N>Y when X ≥ 8 because not all hydroxyls participate in the polymerization due to steric hindrance [11]. The polymers are abbreviated as X-arm PLLA-Y (Table S1). Emulsification and thermally induced phase separation (TIPS) techniques are used to fabricate the microspheres from these SS-PLLAs (Figure 1A). Specifically, glycerol is gradually added (Figure 1A(a, b)) into a 2% (w/v) SS-PLLA/tetrahydrofuran (THF) solution (glycerol : SS-PLLA/THF = 3:1 (v/v)), which causes phase inversion and three types of emulsions to form (Figure 1A(c–e)). The emulsions are then quenched in liquid nitrogen to induce nanometre scale phase separation of the polymer solution (Figure 1A(f)). After glycerol and THF extraction with distilled ice water, the microspheres (Figure 1A(g–i)) are freeze-dried and stored in vacuum.

Nano-scale self-assembly

Quenching the emulsions in liquid nitrogen induces nano-scale phase separation of the polymer solution (Figure 1A(f)). During this thermodynamic process, polymer solutions undergo separation into bi-continuous nanoscale phases (presumably through a spinodal decomposition pathway), SS-PLLA chains rearrange to maximize formation of crystalline domains, and ultimately nanofibres form [12, 13]. According to the Flory-Huggins (FH) theory, the FH polymer-solvent interaction parameter, χ, must exceed a critical value χ_c to trigger the spinodal decomposition pathway [14]. Increasing the molecular weight (MW) of a polymer can reduce χ_c to trigger the spinodal decomposition. In addition to the initiation of the spinodal phase separation, the stabilization of the phase-separated nanofibrous patterns is

needed to obtain nanofibers. It is known that crystallinity of SS-PLLA increases as arm length increases [15]. Therefore, sufficiently long arm length is also needed to crystalize the nanofibers (Table S2). Here, we find that SS-PLLAs assemble into nanofibers only when the arm length N is above a critical value (denoted as N_C) (Figure 1B, C). N_C=~200 when X= 2, 3, 4; $N_C \approx 150$ when X = 8, 16, 32; and $N_C \approx 200$ when X=64 (Table S1). Therefore, an approximate universal N_C (including linear PLLA (with 2 arms) and all the examined SS-PLLAs) appears in the range of 150–200. When $N>N_C$, any SS-PLLA forms nanofibers. Decreasing N leads to fibre aggregation (Figure 1B (middle) and Figure 1C (middle)), and ultimately a smooth (dense) microsphere formation (Figure 1B (left) and Figure 1C (left)).

Micro-scale self-assembly

Prior to nanometre scale phase separation, SS-PLLAs phase separate on the micro-scale during emulsification. Three types of microstructures are identified: non-hollow microspheres (Figure 1A(g)), hollow microspheres with one or multiple pore openings on the shell (Figure 1A(h)), and spongy microspheres with an interconnected pore structure (Figure 1A(i)). This suggests that single emulsions, double emulsions and multiple emulsions are formed, respectively (Figure 1A(c–e)). It should be noted that the hole on the surface of hollow microspheres is caused by the phase inversion process, which connects the encapsulated glycerol and the outer glycerol phase [10]. Combined with the two types of observed nano-scale structure (smooth and nanofibrous), six distinct types of microspheres are formed: smooth non-hollow microspheres, nanofibrous non-hollow microspheres, smooth hollow microspheres, nanofibrous hollow microspheres, smooth spongy microspheres and nanofibrous spongy microspheres (Figure 1D). The characterization of the spheres (porosity, surface area, overall density) is summarized in Table S2. Of particular note is the nanofibrous spongy microsphere, which integrates a nanofibrous structure with an internally interconnected multi-pore structure into microspheres with an increasing number of pores as the diameter increases (Figure 1E).

The values of both X and Y affect the microstructure of the spheres. On the one hand, a small Y favours a more porous microstructure. For example, 16-arm PLLAs transition from non-hollow microspheres to hollow microspheres to spongy microspheres when Y decreases from 700 to 50. Four-arm PLLAs transition from hollow to non-hollow microspheres when Y increases from 300 to 500 (Figure 1F). On the other hand, when Y is fixed, an increased X produces a more porous structure. For instance, when Y= 100, microspheres transition from non-hollow to hollow to spongy as X increases from 2 to 64. We speculate that the hydroxyls of the SS-PLLAs (located at the end of each arm, as well as in the unreacted sites of the initiator core) are responsible for the hollow/spongy structure formation, because the change of the molecular architecture affects the hydroxyl density of the polymers. Here, the hydroxyl density of SS-PLLA, denoted as **OH/LLA**, is calculated from the molar ratio of hydroxyls to monomer LLA. Thus, **OH/LLA**=1/Y. We therefore hypothesize that: 1) the hydroxyl groups are required for the hollow/spongy structure formation, and 2) a high **OH/LLA** value favours the formation of a hollow/spongy structure. Two experiments are designed to test these hypotheses. In the first experiment, we cap the hydroxyls of SS-PLLA prior to emulsification and TIPS (Figure S2a). The hydroxyl-capping reaction “turns off” the polymer’s ability to self-assemble into hollow microspheres. For example, 4-arm PLLA100,

which is capable of forming hollow microspheres (Figure 1D), assembles into non-hollow microspheres after the hydroxyl capping reaction (Figure 2a). This finding supports our first hypothesis that the hydroxyl groups on SS-PLLA are required for the hollow structure formation. In the second experiment, we double **OH/LLA** without altering X or Y (Figure S2b). 4-arm PLLA-400, which has a low **OH/LLA** value (1/400) and forms non-hollow microspheres (Figure 1D), assembles into hollow microspheres after its **OH/LLA** is increased to 1/200 (Figure 2b). 16-arm PLLA-100 (**OH/LLA**=1/100), which forms hollow microspheres (Figure 1D) before modification, assembles into spongy microspheres after hydroxyl doubling (**OH/LLA** increased to 1/50) (Figure 2c). These findings support our second hypothesis that a higher **OH/LLA** favours hollow/spongy structure formation. In these two experiments, the modification does not alter the nanometre scale phase separation, which agrees with our previous discussion that the nanometre scale phase separation is mainly a result of polymer chain-solvent interaction (arm length). Associating the hollow/spongy structure formation with the **OH/LLA** of the SS-PLLAs, we determine the **OH/LLA** threshold values for structural transition of the spheres on the micro-scale (Table S3). Figure 2d shows a phase diagram summarizing the nano-and micro-scale self-assembly as a function of X and Y.

We further hypothesize that the hydroxyl groups of SS-PLLA stabilize the polymer solution/glycerol interface due to the high affinity of hydroxyl to glycerol. As a result, SS-PLLA with a higher **OH/LLA** favours the formation of double/multiple emulsions, which contain larger interfacial area than single emulsions. To test this hypothesis, we perform dissipative particle dynamics (DPD) simulations for 4, 8, and 16 arm polymers and for a range of arm lengths using HOOMD-Blue (http://codeblue.umich.edu/hoomd-blue) [16–18]. For each set of arms, simulations are run for arm lengths of N_{bead} = 10, 40, 80, and 120 coarse grained beads, linked together with harmonic springs. To capture the catastrophic phase inversion process that causes the initial encapsulation of glycerol into the polymer solution droplets (Figure S3), star polymers are initialized within a thin spherical shell. For simplicity, the encapsulated glycerol is not connected to the outer glycerol phase in this simulation study. Each simulation containing between 1.1 and 1.5 million particles is run for at least 5 million time steps to ensure proper equilibration, and additionally verified by running to 50 million time steps for one of each type of microspheres (non-hollow, hollow, and spongy). Larger simulations (containing ~11 million particles, Figure S4) of each type of microsphere are also run to rule out finite size or other non-physical effects. In total, over 100 independent state points are simulated (full details in the simulation section of the **SI**).

For all simulated state points, a transition from hollow to non-hollow is observed as N_{bead} increases, supporting the experimental data. For star-shaped polymers with long arms, the polymer shell ruptures during the simulation and the glycerol mostly leaves the droplet, with only small pockets of solvent remaining inside (Figure 3a, b). For star-shaped polymers with short arms, the double emulsion droplet is stabilized, with the hydroxyl groups concentrated at both the interior and exterior interfaces (Figures 3c, d & S4a, b). By looking at a single star-shaped polymer molecule (Figure 3c), we find that the polymer “stretches” its arms to reach to the interfaces, acting like a surfactant capable of stabilizing both the interior and exterior interfaces. Increasing the strength of attraction between the hydroxyls and glycerol

(mimicking the “hydroxyl doubling” modification experiment) causes a transition from non-hollow to hollow structures, again matching the experimental data (Figure 2b). These results support our hypothesis that hydroxyls can stabilize the interior and exterior interfaces for hollow sphere formation. The high affinity between hydroxyls and glycerol probably stems from their hydrophilic interaction (e.g. hydrogen bonding), which lowers the interfacial tension and stabilizes the interfaces. In addition, for 16-arm polymers with $N_{bead} = 10$, glycerol molecules in the interior of the polymer solution droplet separate into multiple domains (Figures 3e, f & S4c–f), consistent with the experimental finding that 16-arm PLLA with short arms form spongy microspheres (Figure 1D). These simulation results indicate that, while the catastrophic phase inversion might initially cause the encapsulation of glycerol inside the polymer solution droplet (Figure 1A(b)), the final microstructure of the emulsions is determined by **OH/LLA** and the molecular structure of SS-PLLAs.

In summary, star-shaped polymers with varying arm numbers and arm lengths are synthesized, characterized and simulated for the systematic study of their self-assembly during emulsification and TIPS processes. During these processes, phase separation on the nanometre and micrometre scales determines the final structure of the microspheres at these two levels. The nano-scale phase separation of SS-PLLA depends on arm-length, while the micro-scale structure is determined by arm-number and **OH/LLA** ratio. The discovered mechanisms provide guidance on simultaneous control of nano- and micro-structure formation and result in several novel microspheres, which may broadly impact biomedical and other emerging technologies. For example, the interconnected internal pore structure of spongy microspheres may enable deliberate control of cell-cell interactions to maximize regeneration outcome. The nano- and micro-structured spheres may also provide advanced 3D substrates for catalysis or bio-sensing technologies.

Experimental Section

Synthesis of Star-Shaped PLLA

Star-shaped PLLA is prepared via ring-opening polymerization (ROP) of L-lactide. A detailed synthesis procedure can be found in SI. Glycerol, pentaerythritol, *N*,*N*,*N*′,*N*′-tetra(2,3-dihydroxpropyl)ethane-1,2-diamine, PAMAM dendrimers (G2-OH, G3-OH, or G4-OH) are used as the initiators to generate linear PLLA, 3-arm PLLA, 4-arm PLLA, 8-arm PLLA, 16-arm PLLA, 32-arm PLLA, and 64-arm PLLA, respectively. The procedure for capping/doubling of hydroxyl groups are detailed in SI.

Fabrication of Microspheres

The polymer (0.4 g) was dissolved in THF at 50 °C with a concentration of 2% w/v. Under rigorous mechanical stirring (Speed 9, Fisher Science Inc.), glycerol (50 °C) with three times the volume of star-shaped PLLA solution was gradually added into the polymer solution. After stirring for five minutes, the mixture was quickly poured into liquid nitrogen. After 10 min, water-ice mixture (1 L) was added for solvent exchange for 24 h. The microspheres were sieved and washed with distilled water eight times to remove residual glycerol on the sphere surfaces. The spheres were then lyophilized for three days.

DPD Model details

Our DPD model is adapted from past studies of a similar nature [16, 17]. In this model, three forces are applied to each particle (representing the repeating units of the polymer chain) at each time step – a conservative, a random, and a dissipative force. The form and value of all three of these forces are shown in SI, as has been done in prior works [12, 17, 19]. Star polymers are created by linking beads together with harmonic springs to a single polymer core bead. Systems were thermalized for 30 thousand timesteps, and then run for 5 million steps to equilibrate. The amount of solvent was kept fixed at 1 million particles. Four different arm lengths were run: N_{bead} = 10, 40, 80, or 120 beads per arm. All simulations were performed for 4, 8, and 16 arms. In addition, to verify the effect of the hydroxyl stabilizer, two non-hollow cases were tested separately: 8 arm, N_{bead} = 120 at polymer concentrations of both 10% and 13%. The strength of the hydroxyl-solvent and hydroxyl-hydroxyl repulsion was decreased, thereby increasing the preference for the hydroxyls to aggregate at the polymer/solvent interface. In these cases, a hollow to non-hollow transition is triggered when hydroxyl's affinity to glycerol is increased, consistent with the hydroxyl doubling experimental results. Finally, to ensure reproducibility of the structures, three independent runs were conducted for 50 million time steps each using Blue Waters. These runs were also used to create the movies contained in the SI. All simulations were performed using the DPD implementation in HOOMD-Blue, a free and open-source code developed and maintained at the University of Michigan (http:codeblue.umich.edu/hoomd-blue). Images of the droplets and movies were created using VMD, a free visualization package available online. More details about the simulation can be found in SI.

Supplementary Material

Refer to Web version on PubMed Central for supplementary material.

Acknowledgments

The authors gratefully acknowledge financial support from the NIH (NIDCR DE022327, DE015384, and NHLBI HL114038: PXM), DOD (W81XWH-12-2-0008: PXM), and NSF (DMR-1206575: PXM). The simulation work (RLM and SCG) is supported by the U. S. Army Research Office under Grant Award No. W911NF-10-1-0518. Computer resources were provided, in part, by the Blue Waters sustained-petascale computing project, which is supported by the National Science Foundation (awards OCI-0725070 and ACI-1238993) and the state of Illinois. Blue Waters is a joint effort of the University of Illinois at Urbana-Champaign and its National Center for Supercomputing Applications. RLM is grateful to J. Glaser and J. Anderson for discussions regarding DPD simulations.

References

1. Langer R. Nature. 1998; 392:5. [PubMed: 9579855] Barbé C, Bartlett J, Kong L, Finnie K, Lin HQ, Larkin M, Calleja S, Bush A, Calleja G. Advanced Materials. 2004; 16:1959.Zhao W, Chen H, Li Y, Li A, Lang M, Shi J. Advanced Functional Materials. 2008; 18:2780.
2. Comiskey B, Albert JD, Yoshizawa H, Jacobson J. Nature. 1998; 394:253.Shipway AN, Katz E, Willner I. ChemPhysChem. 2000; 1:18. [PubMed: 23696260]
3. Xia Y, Gates B, Yin Y, Lu Y. Advanced Materials. 2000; 12:693.
4. Xia YS, Nguyen TD, Yang M, Lee B, Santos A, Podsiadlo P, Tang ZY, Glotzer SC, Kotov NA. Nature Nanotechnology. 2011; 6:580.
5. Park J Il, Nguyen TD, Silveira GD, Bahng JH, Srivastava S, Zhao GP, Sun K, Zhang PJ, Glotzer SC, Kotov NA. Nature Communications. 2014:5.

6. White SR, Sottos NR, Geubelle PH, Moore JS, Kessler MR, Sriram SR, Brown EN, Viswanathan S. Nature. 2001; 409:794. [PubMed: 11236987]
7. Svec F, Frechet JM. Science. 1996; 273:205. [PubMed: 8662498] Kim SW, Kim M, Lee WY, Hyeon T. Journal of the American Chemical Society. 2002; 124:7642. [PubMed: 12083902] Lee J, Park JC, Song H. Advanced Materials. 2008; 20:1523.
8. Ma PX. Materials Today. 2004; 7:30.Madden LR, Mortisen DJ, Sussman EM, Dupras SK, Fugate JA, Cuy JL, Hauch KD, Laflamme MA, Murry CE, Ratner BD. Proceedings of the National Academy of Sciences. 2010; 107:15211.Hollister SJ. Nature Materials. 2005; 4:518. [PubMed: 16003400]
9. Zhang Z, Hu J, Ma PX. Advanced Drug Delivery Reviews. 2012; 64:1129. [PubMed: 22579758] Zhang S. Nature Biotechnology. 2003; 21:1171.Hartgerink JD, Beniash E, Stupp SI. Science. 2001; 294:1684. [PubMed: 11721046] Kim HW, Song JH, Kim HE. Advanced Functional Materials. 2005; 15:1988.
10. Liu X, Jin X, Ma PX. Nature Materials. 2011; 10:398. [PubMed: 21499313]
11. Zhao Y, Shuai X, Chen C, Xi F. Chemistry of Materials. 2003; 15:2836.
12. Ma PX, Zhang R. Journal of biomedical materials research. 1999; 46:60. [PubMed: 10357136]
13. Marson RL, Phillips CL, Anderson JA, Glotzer SC. Nano Letters. 2014; 14:2071. [PubMed: 24641517]
14. Flory PJ. The Journal of Chemical Physics. 1941; 9:660.
15. Zhang W, Zheng S. Polymer Bulletin. 2007; 58:767.
16. Groot RD, Warren PB. Journal of Chemical Physics. 1997; 107:4423.
17. Phillips CL, Anderson JA, Glotzer SC. Journal of Computational Physics. 2011; 230:7191.
18. Anderson JA, Lorenz CD, Travesset A. Journal of Computational Physics. 2008; 227:5342.
19. Jens Glaser TDN, Anderson Joshua A, Lui Pak, Spiga Filippo, Millan Jaime A, Morse David C, Glotzer Sharon C. 2014 arXiv.

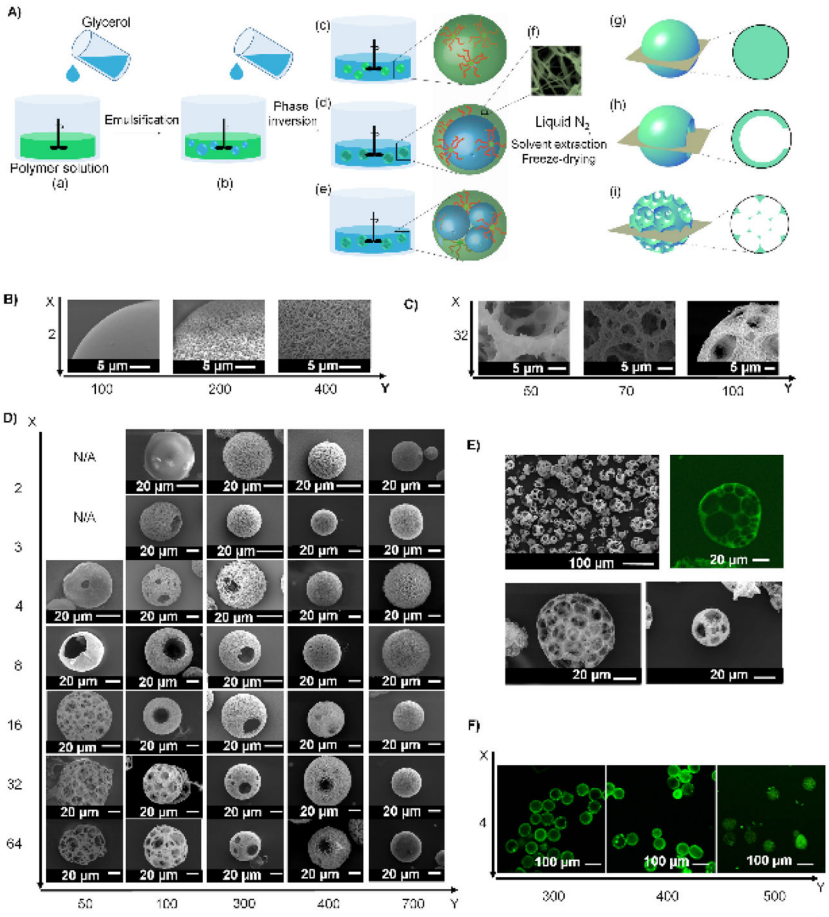

Figure 1. (A) An illustration of the combination of emulsification and thermally-induced phase separation to fabricate nano- and micro-structured spheres

(a, b) Glycerol is slowly poured into a stirred polymer solution. **(c–e)** As the amount of the added glycerol increases, catastrophic phase inversion occurs, generating three types of emulsions: **(c)** a single emulsion (simple polymer droplets); **(d)** a double emulsion (one inner droplet of glycerol inside one polymer droplet); and **(e)** an emulsion with multiple inner droplets of glycerol inside one polymer droplet (referred as “multiple emulsion” hereafter). **(f)** Emulsions are quenched in liquid nitrogen to induce phase separation on the nanometre scale. Upon solvent/glycerol extraction and freeze-drying, **(g)** the single emulsions form non-hollow microspheres; **(h)** the double emulsions form hollow microspheres; and **(i)** the multiple emulsions form spongy microspheres. **(B–F) Structural characterization of microspheres fabricated from SS-PLLA of different X and Y. B–D)** SEM micrographs of microspheres fabricated from **(B)** 2-arm PLLAs with Y= 100, 200 and 400. Scale bars: 5 μm; **(C)** 32-arm PLLAs with Y= 50, 70 and 100. Scale bars: 5 μm; **(D)** SS-PLLAs of different X and Y, showing the structural transition process as X and Y changes. Scale bars: 20 μm. **(E)** SEM and cross-sectional confocal images of microspheres formed from 32-arm PLLA-100. Scale bars: 100 μm in top left panel and 20 μm in the rest of the panels; **(F)** Cross-sectional confocal images of microspheres fabricated from 4-arm PLLAs with Y= 300, 400 and 500. Scale bars: 100 μm.

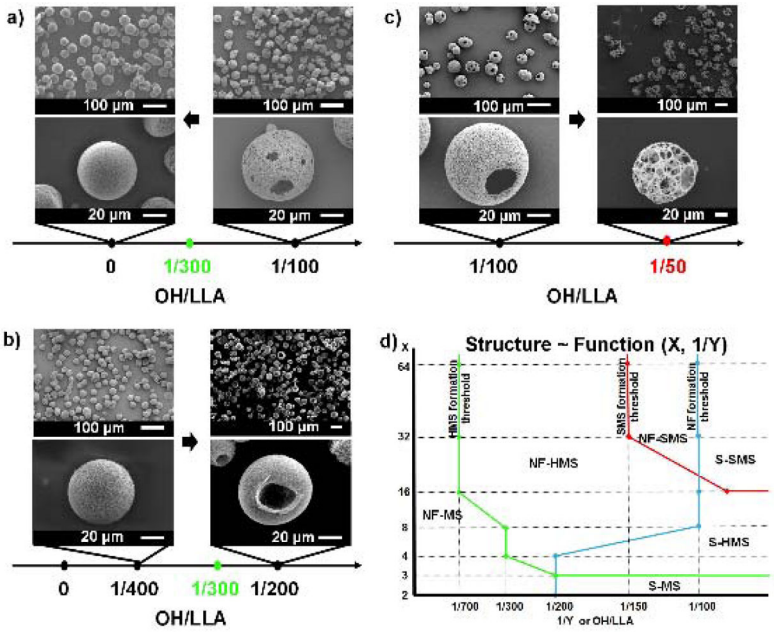

Figure 2. Hydroxyl density of SS-PLLA affects the micro-scale structure of microspheres

a–c) SEM micrographs of microspheres fabricated from **a)** 4-arm PLLA-100 before (right column) and after (left column) hydroxyl capping. **b)** 4-arm PLLA-200 before (left column) and after (right column) hydroxyl doubling. **c)** 16-arm PLLA-100 before (left column) and after (right column) hydroxyl doubling. The hollow-to-non-hollow transition point is 1/300 for 4-arm PLLAs. The hollow-to-spongy transition point for 16-arm PLLAs is 1/50. Scale bars: 100 μm on the top row, 20 μm on the bottom row. **d)** The structure of microspheres as a function of arm number and arm length. Note: This graph is based on SS-PLLAs without modification. S-MS refers to smooth non-hollow microspheres, NF-MS refers to nanofibrous non-hollow microspheres, S-HMS refers to smooth hollow microspheres, NF-HMS refers to nanofibrous hollow microspheres, S-SMS refers to smooth spongy microspheres, NF-SMS refers to nanofibrous spongy microspheres. As 1/Y and X increase, the transition from MS to HMS is represented by the green line (line on MS), while the transition from HMS to SMS is indicated by the red line (line on SMS). As 1/Y decreases and X increases, the transition from S into NF is represented by the blue line (line on NF).

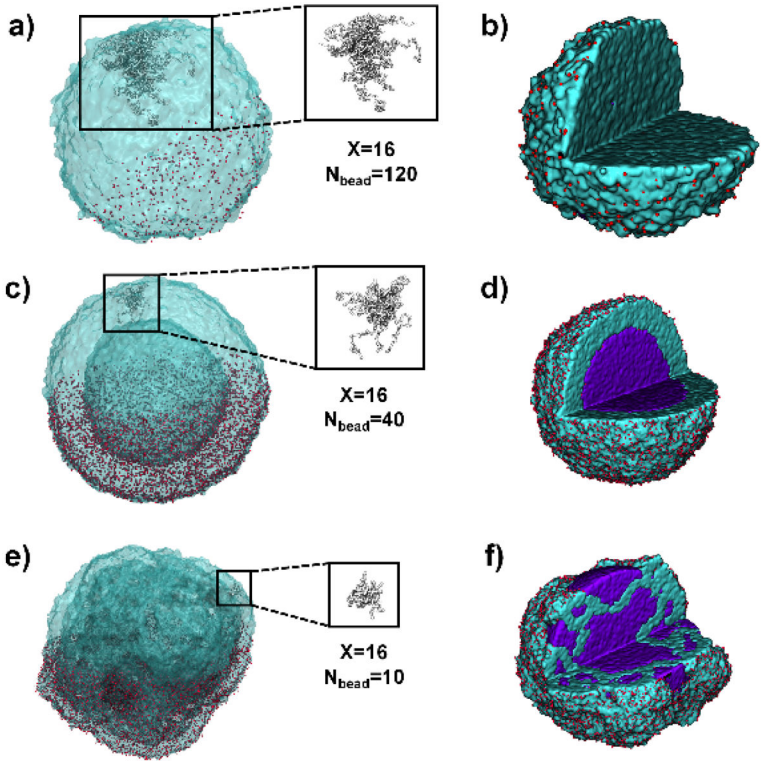

Figure 3. DPD simulations of 16-arm star-shaped polymers of varying arm lengths and the formation of different emulsions

For 16-arm PLLAs, as the length of the polymer arm decreases from 120 to 10, the structures undergo a transition from non-hollow (N_{bead}=120, **a, b**) to hollow (N_{bead}=40, **c, d**) to spongy (N_{bead}=10, **e, f**). This occurs for a variety of polymer droplet concentrations and in other star polymer systems with different arm numbers. The left column of images **(a, c, e)** shows the polymer isosurface, with individual hydroxyl beads on the bottom half of the droplet shown in red. The conformation of a single 16-arm PLLA is shown in the square box. The right column **(b, f, j)** shows the internal structure of the same droplet in the left, with glycerol in purple. Some hydroxyls (red beads) are removed for clarity.